

RSC Advances



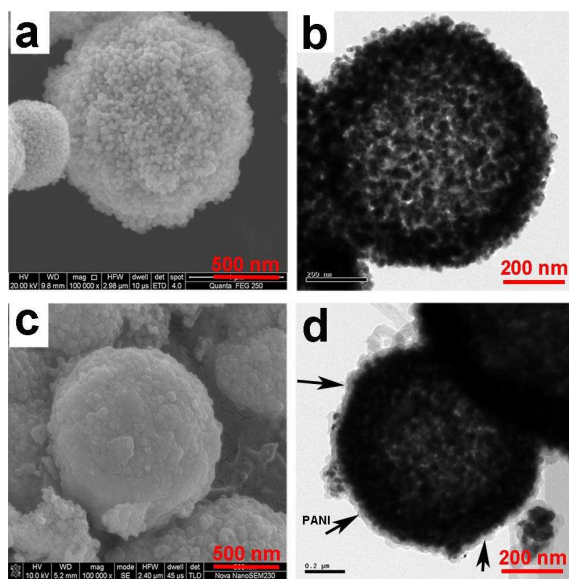
This is an *Accepted Manuscript*, which has been through the Royal Society of Chemistry peer review process and has been accepted for publication.

Accepted Manuscripts are published online shortly after acceptance, before technical editing, formatting and proof reading. Using this free service, authors can make their results available to the community, in citable form, before we publish the edited article. This *Accepted Manuscript* will be replaced by the edited, formatted and paginated article as soon as this is available.

You can find more information about *Accepted Manuscripts* in the [Information for Authors](#).

Please note that technical editing may introduce minor changes to the text and/or graphics, which may alter content. The journal's standard [Terms & Conditions](#) and the [Ethical guidelines](#) still apply. In no event shall the Royal Society of Chemistry be held responsible for any errors or omissions in this *Accepted Manuscript* or any consequences arising from the use of any information it contains.

Graphical abstract



Core-shell structured SnO_2 hollow spheres-polyaniline composites have been synthesized by in-situ polymerization of aniline monomers in the presence of SnO_2 hollow spheres prepared by two-step hydrothermal method and thermal treatment. Using as anode material for sodium-ion batteries, the SnO_2 @PANI composites exhibit long cycle life and good rate capability.

Core-shell structured SnO₂ hollow spheres-polyaniline composites as anode for sodium-ion batteries

Xingxing Zhao, Zhian Zhang*, Fuhua Yang, Yun Fu, Yanqing Lai, and Jie Li

School of Metallurgy and Environment, Central South University, Changsha 410083,

China

Abstract

Core-shell structured SnO₂ hollow spheres (designated as SnO₂-HS)-polyaniline (PANI) composites (SnO₂@PANI) have been synthesized by in-situ polymerization of aniline monomers in the presence of SnO₂-HS prepared by two-step hydrothermal method and thermal treatment. Using as anode materials for sodium-ion batteries (SIBs), the SnO₂@PANI composites exhibit long cycle life and good rate capability. SnO₂@PANI composites are able to deliver a relatively high reversible capacity of 213.5 mA h g⁻¹ after 400 cycles at 300 mA g⁻¹, while bare SnO₂ particles anode only can deliver a much lower capacity of 14.4 mA h g⁻¹ after 400 cycles at the same current density. The enhanced electrochemical performance could be ascribed to the unique hollow structure and the PANI buffer layer, which are found to be beneficial for decreasing the likelihood of pulverization of SnO₂ and agglomeration of generated Sn particles during the discharge and charge process.

Introduction

Rechargeable lithium ion batteries (LIBs) are currently predominant energy storage systems and show promising applications in large scale electrical energy storage such as electric vehicles (EVs) and hybrid electric vehicles (HEVs).¹⁻⁴ However, there is a growing concern on the cost and limitation of lithium reserves for large-scale commercial application besides the reliability and safety problem.⁵⁻⁸ Based on the high availability and fairly low cost of sodium, sodium-ion batteries (SIBs) have gained recognition as a more and more attractive electrochemical power source which have the potential of meeting large scale electrical energy storage needs.⁹⁻¹⁴

Since Na⁺ ion (0.102 nm) is about 40% larger than Li⁺ ion (0.076 nm) in radius, so it is more difficult to find a appropriate host material for reversible Na-ion batteries.¹²

Hence, finding and optimizing suitable anode materials is one of the crucial issues for the development of Na-ion batteries. In order to cope with this challenge, a large variety of anode materials including various carbonaceous materials,¹⁵⁻¹⁸ intermetallic anode materials,¹⁹⁻²¹ metal oxide²²⁻²⁴ have been explored. Among these metal oxides investigated as electrode materials, SnO₂ receives a special attention because SnO₂ can yield a theoretical reversible specific capacity of 667 mA h g⁻¹, in addition to its environmental benignity and quite low cost.²⁵ However, SnO₂ exhibits relatively bad rate capacity and poor cycling performance because of the extremely large volume expansion during the sodium insertion-extraction process. To solve this problem, an enormous amount of research efforts go into optimization of tin oxides. Kushima et al. explored the chemical and structural evolution of SnO₂ nanowire in SIBs by

transmission electron microscopy and density functional theory calculations.²⁶ Xie et al. synthesised SnO₂@graphene nanocomposites through a hydrothermal route as an anode candidate for SIBs with a capacity of 324 mA h g⁻¹ at 50 mA g⁻¹.²⁷ Wang et al. prepared SnO₂@multiwalled carbon nanotubes by a solvothermal method, which delivered a capacity of 230 mA h g⁻¹ at 250 mA g⁻¹ over 50 cycles.²⁸

In addition to preparing SnO₂/C composites for improving the capacity retention, designing and synthesizing unique SnO₂ morphology has been turned out to be an efficacious method to enhance the cyclic stability in LIBs, such as nanorod arrays,²⁹ nanotubes,³⁰ and hollow nanostructures.³¹⁻³³ On the other hand, conducting polymers have also been introduced to improve the anode performance in LIBs. In addition to improving electron conductivity, the soft polymer matrix also can relax the internal stress of solid particle that suffer from severe volume change during charge and discharge cycles.³⁴ Polyaniline (PANI) has gained comprehensive attentions as one of the conducting polymers, due to its environmental stability and easy synthesis.

Herein, we report a core-shell structured SnO₂ hollow spheres-polyaniline composites, in which SnO₂-HS were prepared by two-step hydrothermal method and thermal treatment. The proposed synergistic effect between the PANI shell and the hollow structure can alleviate the volume changes of SnO₂ and agglomeration of generated Sn particles during the discharge and charge process, and therefore improve electrochemical performance of SnO₂ anode materials in SIBs. The SnO₂@PANI composites exhibit long cycle life and good rate performance, delivering a high discharge capacity of 213.5 mA h g⁻¹ over 400 cycles at 300 mA g⁻¹.

Experimental

Preparation of SnO₂ hollow spheres

The SnO₂ hollow spheres (SnO₂-HS) were synthesized by a simple hydrothermal method in aqueous glucose/SnCl₄ solution via self-assembly method. The typical procedure is first to dissolve 4.28 g of glucose and 4.38 g of SnCl₄•5H₂O in ethanol (30 mL) and deionized water (15 mL) to obtain a transparent colorless solution by magnetic stirring. The mixed solution was then transferred into a Teflon-lined stainless steel autoclave (60 mL). Then the autoclave was kept at 180 °C for 24 h before it was cooled in air. The black sediment obtained was filtered and washed with ethanol and deionized water, and finally dried in a vacuum oven at 80 °C for a few hours. Subsequently, the sediment was calcined in air at 650 °C for 5 h to burn off carbon, leaving SnO₂ hollow microspheres (SnO₂-HS). The black sediment turned light yellow indicating the successful removal of carbon by oxidization in air. Bare SnO₂ particles were also synthesized through the above procedure but without adding glucose.

Preparation of core-shell structured SnO₂ hollow spheres-polyaniline composites

The SnO₂-HS were covered by a PANI shell via in-situ chemical polymerization route. In a typical procedure, 0.5 g of SnO₂-HS were uniformly dispersed in a 80 mL aqueous solution containing 8 mg of cetrimonium bromide(CTAB) under sonication for 30 min and magnetic stirring for 3 h. After magnetic stirring, 0.7 mL aniline monomer was slowly added into the above solution under stirring. Then, 20 mL of 0.1 M ammonium persulfate(APS) aqueous solution was dropwise added into the solution.

The gradually changing color from light gray to black indicated the formation of PANI. The polymerization process was conducted with stirring continuously for 4 h at room temperature. The resulting black products were washed and centrifugated with ethanol and deionized water at least three times, and then dried at 60 °C under vacuum overnight.

Materials characterization

The morphologies of the as-prepared materials were observed by field emission scanning electron microscopy (FESEM, Nova NanoSEM 230) and transmission electron microscopy (TEM, TecnaiG2 20ST). Powder X-ray diffraction (XRD, Rigaku 3014) using Cu Ka radiation was employed to identify the phase of the hydrothermal products. Thermo gravimetric analysis (TGA, SDTQ600) was also measured in determining the tin oxide content in the SnO₂@PANI composites. TGA measurement was performed from 25 °C to 800 °C at a heating rate of 5 °C min⁻¹ in air.

Electrochemical measurements

The electrodes were fabricated by a slurry coating process. The anode slurry was prepared by mixing 80 wt% core-shell structured SnO₂ hollow spheres-polyaniline composites, 10 wt% acetylene black and 10 wt% carboxymethyl cellulose (CMC) binder in water by grinding. The slurry of the anode was casted onto a copper foil, then dried overnight at 55 °C under vacuuming. The same method was also used to fabricate the SnO₂ hollow spheres and bare SnO₂ anodes. The electrochemical properties were measured by assembling a CR-2025 type coin cell with a sodium metal sheet as the counter and reference electrode in an argon-filled glove box

(Universal 2440/750) in which water and oxygen contents were both no more than 2 ppm. The electrolyte used was 0.8 M NaClO₄ dissolved in a mixture of diethyl carbonate (DEC)/ethylene carbonate (EC) (1:1 in v/v) with 5 wt% fluoroethylene carbonate (FEC) additive. Cyclic voltammetry (CV) and electrochemical impedance spectroscopy (EIS) measurements were both carried out on the PARSTAT 2273 electrochemical measurement system. CV tests were performed in the voltage range of 0.01-2.0 V at a scan rate of 0.2 mV s⁻¹. The galvanostatic charge/discharge tests were evaluated at a current density of 300 mA g⁻¹ with a cut-off voltage range from 0.01-2.0 V under a LAND CT 2001A charge/discharge system.

Results and discussion

Synthesis and characterization

The schematic illustration in Fig. 1 displays the overall experimental procedure of preparing SnO₂@PANI composites. Firstly, carbon spheres could be synthesized by facile solvothermal process in aqueous glucose solution³⁵. Meanwhile, the SnCl₄ salts hydrolyzed and dehydrated to form SnO₂ particles. Then the SnO₂ particles were anchored on the surface of the pre-synthesized carbon spheres. Subsequently, SnO₂ hollow spheres could be gained by getting rid of the inner carbon templates by calcinations in air. Collectively this had led to the formation of hollow spheres consisting entirely of aggregates of crystalline SnO₂ nanoparticles. Finally, the SnO₂ hollow spheres were covered by a PANI shell via an in-situ chemical polymerization route.

Fig. 2a shows the XRD patterns of PANI, SnO₂-HS, and SnO₂@PANI composites. All

of the diffraction peaks of SnO₂-HS could be consistently indexed on the SnO₂ phase with a tetragonal rutile structure (JCPDS card no. 41-1445). However, PANI simply has a weak and broad diffraction centered at 23°, indicating a poorly crystalline state. In comparison with SnO₂-HS, the SnO₂@PANI composites showed sharp peaks of SnO₂ with reduced peak intensity and no peak shift, which suggesting absence of phase transformations during in situ chemical polymerization. As shown in Fig. 2b, thermo gravimetric analysis was used to determine the amount of PANI and SnO₂ in the SnO₂@PANI composites. The TGA analysis indicates that the PANI content in the composites is 28.06 wt% and the SnO₂ content is 71.94 wt%.

Morphologies of the materials were revealed by SEM and TEM images, as shown in Fig. 3. The SEM images of the SnO₂ hollow spheres at different magnifications are presented in Fig. 3b and 3d. As shown in Fig. 3a, 3b and 3d, the SnO₂-HS exhibit a uniform and rather spherical shape with diameters in the range of 400-1000 nm. Furthermore, it can be seen that the SnO₂-HS have a rough and porous morphology being composed of numerous SnO₂ nanoparticles. Typical TEM images of SnO₂-HS at different magnifications (Fig. 3c and 3e) reveal that the SnO₂-HS have a hollow structure which has a large internal void space. The SEM image of SnO₂@PANI composites (Fig. 3g), shows that the surface of SnO₂@PANI composites is more smooth compared with Fig. 3d, indicating that SnO₂-HS have been wrapped by PANI coatings. Meanwhile, Fig. 3h shows representative TEM image of SnO₂@PANI, from which the PANI layer coated on SnO₂-HS is observed to be approximately 15-20 nm (marked by an arrow). Moreover, HR-TEM image in Fig. 3e and 3i, show an

interplanar spacing of about 0.335 nm and 0.268 nm (corresponding to the (110) and (101) planes of SnO₂) and a PANI layer clearly, indicating the formation of SnO₂@PANI.

Electrochemical performance

Fig. 4a shows the cyclic voltammetry (CV) curves of the SnO₂@PANI composites anode for three cycles. The discharge and charge reactions can be modified as follows: $\text{SnO}_2 + 4\text{Na} \rightarrow \text{Sn} + 2\text{Na}_2\text{O}$ (1), $\text{Sn} + x\text{Na} \leftrightarrow \text{Na}_x\text{Sn}$ (2).²⁵ During the first discharge, a large irreversible reaction between 0.5 V and 1.0 V can be observed, which is associated with the irreversible reaction of SnO₂ with Na⁺ ion to form metallic Sn and amorphous Na₂O and the decomposition of the electrolyte. These weak oxidation peaks can be assigned to the reversible dealloying of Na_xSn. From the second cycle, all redox peaks are well overlapped, indicating high electrochemical reversibility of the SnO₂@PANI electrode. Fig. 4b shows the charge and discharge curves of the first three cycles. In consistence with the CV profiles, the initial discharge profiles show an irreversible plateau at around 0.75 V. This plateau just appears in the first cycle and can be ascribed to the irreversible reaction of SnO₂ with Na⁺ to form Sn and Na₂O along with the formation of a solid-electrolyte interface (SEI) layer. Upon charge, the reaction is reversed. A large decrease of the discharge capacity between the initial cycle and the second cycles is visible. The irreversible capacity loss in the first charge and discharge process is mainly attributed to the irreversible reaction (1) and the formation of a SEI film on the surface of the anode.^{36,37} The discharge and charge curves remains almost unchanged from the

second cycle, suggesting good reversibility.

Fig.5a shows the cycling performances of SnO₂-HS, bare SnO₂ particles and SnO₂@PANI composites. As shown in Fig. 5a, the bare SnO₂ particles anode delivers a specific capacity of 508.3 mA h g⁻¹ during the initial discharge but retains only 14.4 mA h g⁻¹ after 400 cycles at 300 mA g⁻¹. By contrast, the retained specific capacity for the SnO₂-HS anode is 145.5 mA h g⁻¹ in the 400th cycle, while the SnO₂@PANI (28.06 wt%) core-shell composites anode can deliver an initial specific capacity of 667.8 mA h g⁻¹ and keep 213.5 mA h g⁻¹ after 400 cycles at the same current density. SnO₂@PANI composites exhibit a much higher sodium storage capability than that of SnO₂-HS, bare SnO₂ particles, those of previously reported SnO₂/C materials^{27,28} and carbonaceous materials.^{38,39} Wang et al. prepared SnO₂@multiwalled carbon nanotubes through a solvothermal method, whose discharge capacity decrease to 230 mA h g⁻¹ at 250 mA g⁻¹ only after 50 cycles.²⁸ White et al. synthesized hollow carbon nanospheres by template method as sodium ion battery anode material. After 100 cycles, only 160 mA h g⁻¹ is stably attained.³⁹ The SnO₂@PANI composites anode also displays similar discharge profiles in the following cycles (the inset in Fig. 5a), indicating a good reversibility of the SnO₂@PANI composites anode. We also tested the rate capabilities of SnO₂@PANI composites at varied current densities from a current density of 50 mA g⁻¹ up to 1000 mA g⁻¹ (Fig. 5b). It is clear showed that the SnO₂-HS anode presents much lower capacity than the SnO₂@PANI composites electrode at different current rates. When cycling at 1000 mA g⁻¹, the SnO₂@PANI still can deliver a capacity of about 110 mA

h g⁻¹. The specific discharge capacity can quickly recover to 235 mA h g⁻¹ as the current density reversed back from 1000 mA g⁻¹ to 200 mA g⁻¹. This approves that SnO₂@PANI composites are tolerant to varied discharge current densities.

In order to comprehend the different electrochemical behaviors, EIS of SnO₂-HS and SnO₂@PANI was further carried out as shown in Fig. 6. The Nyquist plots were fitted by the equivalent circuit. As shown in Fig. 6, where Re represents electrolyte and ohm resistance, R_{int} and C1 represent surface film resistance and the relax capacitance, R_{ct} and C2 represent the charge transfer resistance and the double layer capacitance, and W_o is the Na-ion bulk diffusion resistance. Base on the equivalent circuit fitting, SnO₂/PANI composites exhibit a much lower R_{ct} value (683.5Ω) than bare SnO₂-HS (964.4Ω). The conducting effect of PANI is responsible for the lower R_{ct} value of SnO₂/PANI composites. On the basis of these results, it confirms that the incorporation of PANI coating is an effective method for enhancing the electron transport of SnO₂-HS, which leads to an improvement in the electrochemical performance.

The enhanced electrochemical performance can be attributed to the synergistic effect of the PANI shell and the SnO₂-HS, which is able to mitigate the large volume change of SnO₂ during charge and discharge progress and prevent the nanoparticles from agglomerating. A probable mechanism of this synergistic effect, in which the PANI shell can act as a buffer to alleviate the volume change of SnO₂ hollow spheres, is put forward in Fig. 7. During the discharge process, SnO₂ nanoparticles would react with Na to form a mixture of Na₂O and Na_xSn, as shown in reaction (1) and (2).

Subsequently, metallic Sn and Na is converted from the Na_xSn dealloying process during sodium extraction. The effects of the great volume change of SnO_2 can be mitigated by the PANI coating, which serves as a buffer between contiguous SnO_2 -HS. Furthermore, the large inner hollow space can accommodate the great volume change to some extent. Hence, the proposed synergistic effect between the PANI shell and the hollow structure of SnO_2 -HS can decrease the likelihood of pulverization of the SnO_2 anode electrode. In addition, the PANI shell is also able to provide good electrical contact within the composites, which is in agreement with the results of EIS.

In order to confirm the proposed mechanism, morphological study of bare SnO_2 and SnO_2 @PANI core-shell composites electrode after cycling 400 cycles were studied by SEM and TEM. Fig. 8a and 8b show that the cracks in the bare SnO_2 anode after 400 cycles are much larger than that in the SnO_2 @PANI composites anode. And in Fig. 8c and 8d, some deformation of hollow spheres structure is observed, but the entire sphere structure is maintained and each hollow sphere is interconnected. The results indicate that the PANI buffer on SnO_2 -HS and large inter space have the ability to alleviate the large volume expansion and maintain the structural integrity of the anode.

Conclusions

In this work, core-shell structured SnO_2 hollow spheres-polyaniline composites (SnO_2 @PANI) have been synthesized through in-situ polymerization of aniline monomers in the presence of preprepared SnO_2 -HS. The SnO_2 @PANI composites is successfully used as an anode material for SIBs, exhibiting significantly enhanced

cycling performance (213.5 mAh g^{-1} after 400 cycles) and good rate performance. The enhanced cycling performance is attributed to the unique hollow structure and the PANI buffer layers, which are found to be beneficial for alleviating the volume changes of SnO_2 and agglomeration of generated Sn particles during the discharge and charge process. This work may open a new path toward designing SnO_2 based composites anode materials for Na-ion batteries with improved cyclic stability. In addition, the formation of the stable SEI film on the surface of anode also contributes to the good electrochemical performance of $\text{SnO}_2@\text{PANI}$ by stabilizing the electrode/electrolyte interface.

Acknowledgements

The authors acknowledge that this work was supported by Teacher Research Fund of Central South University (2013JSJJ027).

Notes and references

1. J. M. Tarascon and M. Armand, *Nature*, 2001, **414**, 359.
2. J. B. Goodenough and Y. Kim, *Chem. Mater.*, 2010, **22**, 587.
3. B. Scrosati, J. Hassoun and Y. Sun, *Energy Environ. Sci.*, 2011, **4**, 3287.
4. T. H. Kim, J. S. Park, S. K. Chang, S. Choi, J. H. Ryu and H. K. Song, *Adv. Energy Mater.*, 2012, **2**, 860.
5. J. M. Tarascon, *Nat. Chem.*, 2010, **2**, 510.
6. B. Dunn, H. Kamath and J. M. Tarascon, *Science*, 2011, **334**, 928.
7. V. Etacheri, R. Marom, R. Elazari, G. Salitra and D. Aurbach, *Energy Environ. Sci.*, 2011, **4**, 3243.
8. M. M. Thackeray, C. Wolverton and E. D. Isaacs, *Energy Environ. Sci.*, 2012, **5**, 7854.
9. D. A. Stevens and J. R. Dahn, *J. Electrochem. Soc.*, 2000, **147**, 1271.
10. S. Komaba, W. Murata, T. Ishikawa, N. Yabuuchi, T. Ozeki, T. Nakayama, A. Ogata, K. Gotoh and K. Fujiwara, *Adv. Funct. Mater.*, 2011, **21**, 3859.
11. V. Palomares, P. Serras, I. Villaluenga, K. B. Hueso, J. C. Gonzalez and T. Rojo, *Energy Environ. Sci.*, 2012, **5**, 5884.
12. S. P. Ong, V. L. Chevrier, G. Hautier, A. Jain, C. Moore, S. Kim, X. H. Ma and G. Cedar, *Energy Environ. Sci.*, 2011, **4**, 3680.
13. D. Kim, S. H. Kang, M. Slater, S. Rood, J. T. Vaughey, N. Karan, M. Balasubramanian and C.

- S. Johnson, *Adv. Energy Mater.*, 2011, **1**, 333.
14. Y. L. Cao, L. F. Xiao, W. Wang, D. W. Choi, Z. M. Nie, J. G. Yu, L. V. Saraf, Z. G. Yang and L. Jun, *Adv. Mater.*, 2011, **23**, 3155.
 15. R. C. Asher and S.A. Wilson, *Nature*, 1958, **181**, 409.
 16. P. Thomas, J. Ghanbaja and D. Billaud, *Electrochim. Acta*, 1999, **45**, 423.
 17. Y. Yan, Y. X. Yin, Y. G. Guo and L. J. Wan, *Adv. Energy Mater.*, 2014, **4**, 1301584.
 18. Y. X. Wang, S. L. Chou, H. K. Liu and S. X. Dou, *Carbon*, 2013, **57**, 202.
 19. Y. C. Liu, N. Zhang, L. F. Jiao, Z. L. Tao and J. Chen, *Adv. Funct. Mater.*, 2014, DOI: 10.1002/adfm.201402943.
 20. L. Wu, X. H. Hu, J. F. Qian, F. Pei, F. Y. Wu, R. J. Mao, X. P. Ai, H. X. Yang and Y. L. Cao, *Energy Environ. Sci.*, 2014, **7**, 323.
 21. B. Farbod, K. Cui, W. P. Kalisvaart, M. Kupsta, B. Zahiri, A. Kohandehghan, E. M. Lotfabad, Z. Li, E. J. Luber and D. Mitlin, *ACS Nano.*, 2014, **8**, 4415.
 22. S. Hariharan, K. Saravanan, V. Ramar and P. Balaya, *Phys. Chem. Chem. Phys.*, 2013, **15**, 2945.
 23. Y. Liu, B. H. Zhang, S. Y. Xiao, L. L. Liu, Z. B. Wen and Y. P. Wu, *Electrochim. Acta*, 2014, **116**, 512.
 24. J. Kong, Y. Wei, C. Zhao, M. Y. Toh, W. A. Yee, D. Zhou, S. L. Phua, Y. Dong and X. Lu, *Nanoscale*, 2014, **6**, 4352.
 25. Y. X. Wang, Y. G. Lim, M. S. Park, S. L. Chou, J. H. Kim, H. K. Liu, S. X. Dou and Y. J. Kim, *J. Mater. Chem. A*, 2014, **2**, 529.
 26. M. Gu, A. Kushima, Y. Shao, J. G. Zhang, J. Liu, N. D. Browning, J. Li and C. M. Wang, *Nano Lett.*, 2013, **13**, 5203.
 27. Y. Zhang, J. Xie, S. Zhang, P. Zhu, G. Cao and X. Zhao, *Electrochim. Acta*, 2014, DOI: <http://dx.doi.org/doi:10.1016/j.electacta.2014.11.009>.
 28. Y. Wang, D. Su, C. Wang, G. Wang, *Electrochem. Commun.*, 2013, **29**, 8.
 29. D. Lei, M. Zhang, Q. Hao, L. Chen, Q. Li, E. Zhang and T. Wang, *Mater. Lett.*, 2011, **65**, 1154.
 30. L. Li, X. Yin, S. Liu, Y. Wang, L. Chen and T. Wang, *Electrochem. Commun.*, 2010, **12**, 1383.
 31. X. W. Lou, Y. Wang, C. Yuan, J. Y. Lee and L. A. Archer, *Adv. Mater.*, 2006, **16**, 2325.
 32. X. M. Yin, C. C. Li, M. Zhang, Q. Y. Hao, S. Liu, L. B. Chen and T. H. Wang, *J. Phys. Chem. C*, 2010, **114**, 8084.
 33. R. Q. Liu, D. Y. Li, C. Wang, N. Li, Q. Li, X. J. Lü, J. S. Spendelow and G. Wu, *Nano Energy*, 2014, **6**, 73.
 34. L. Cui, J. Shen, F. Cheng, Z. Tao and J. Chen, *J. Power Sources*, 2011, **196**, 2195.
 35. Q. Wang, H. Li, L. Chen and X. Huang, *Carbon*, 2001, **39**, 2211.
 36. L. F. Xiao, Y. L. Cao, J. Xiao, W. Wang, L. Kovarik, Z. M. Nie and J. Liu, *Chem. Commun.*, 2012, **48**, 3321.
 37. L. Noerochim, J. Z. Wang, S. L. Chou, D. Wexler and H. K. Liu, *Carbon*, 2012, **50**, 1289.
 38. K. Tang, L. Fu, R. J. White, L. Yu, M. M. Titirici, M. Antonietti and J. Maier, *Adv. Energy Mater.*, 2012, **2**, 873.
 39. Y. X. Wang, S. L. Chou, H. K. Liu and S. X. Dou, *Carbon*, 2013, **157**, 202.

Figures and figure captions

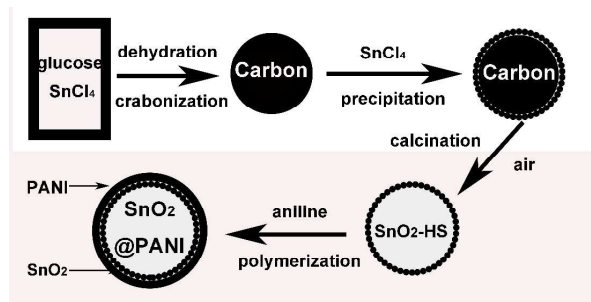


Fig. 1 Schematic illustration of the formation processes of the SnO₂-HS and SnO₂@PANI.

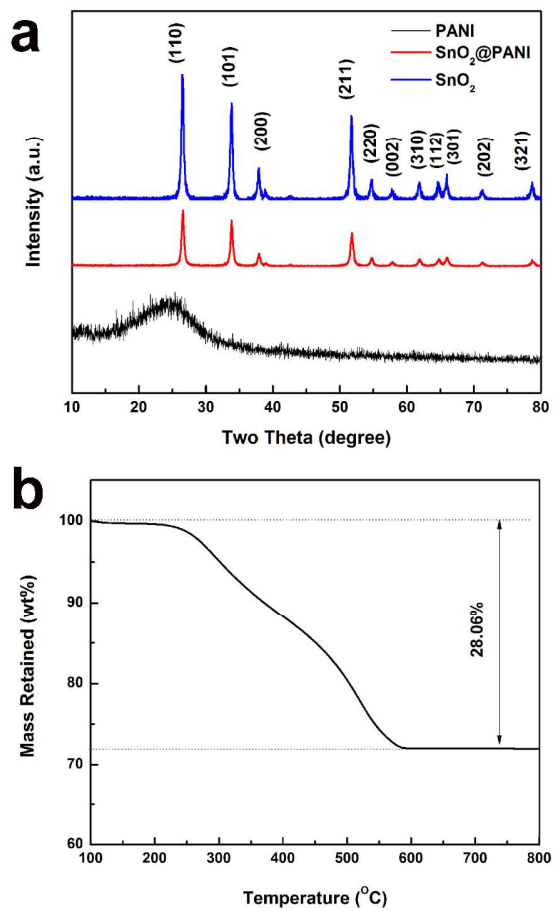


Fig. 2 (a) XRD patterns of bare SnO₂, PANI, and SnO₂@PANI, (b) TGA curves of SnO₂@PANI composites.

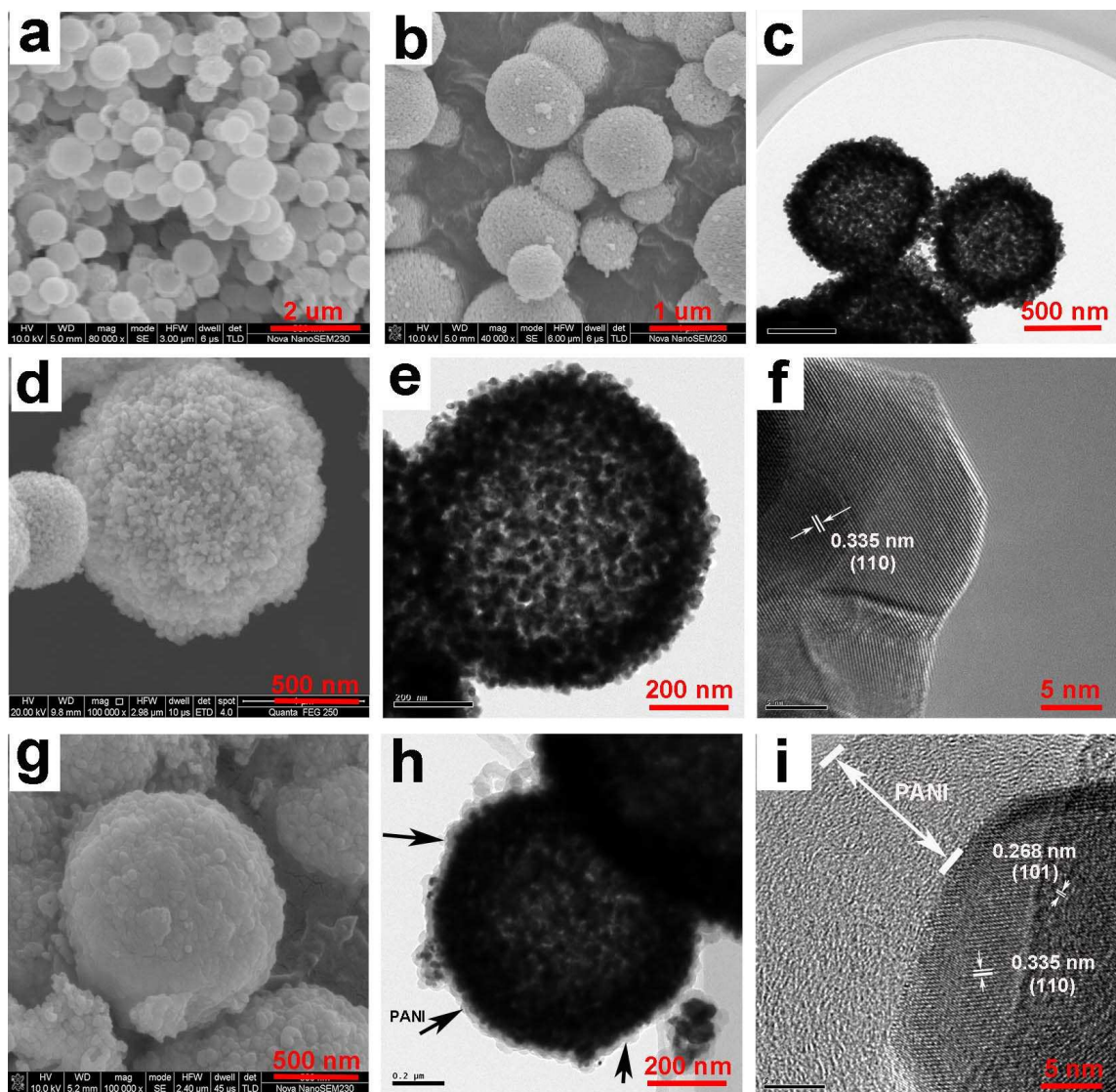


Fig. 3 SEM images of SnO₂-HS (a) (b) and (d), SnO₂@PANI (g), at different magnifications; TEM images of SnO₂-HS (c) and (e), SnO₂@PANI (h); HR-TEM images of SnO₂-HS (f), SnO₂@PANI (i).

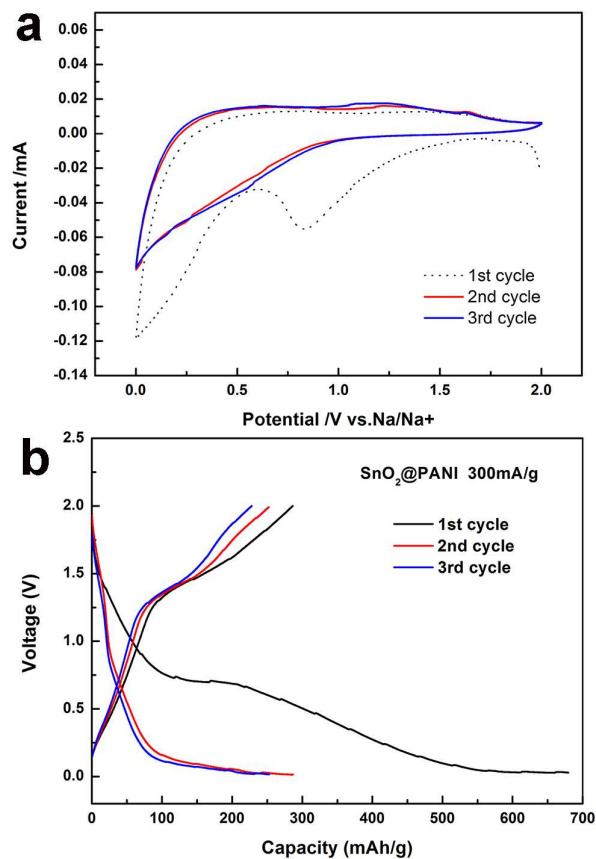


Fig. 4 (a) Cyclic voltammograms of SnO₂@PANI for the first 3 cycles at 0.2 mV s⁻¹;
(b) Discharge and charge profiles of SnO₂@PANI for the first 3 cycles at 300 mA g⁻¹.

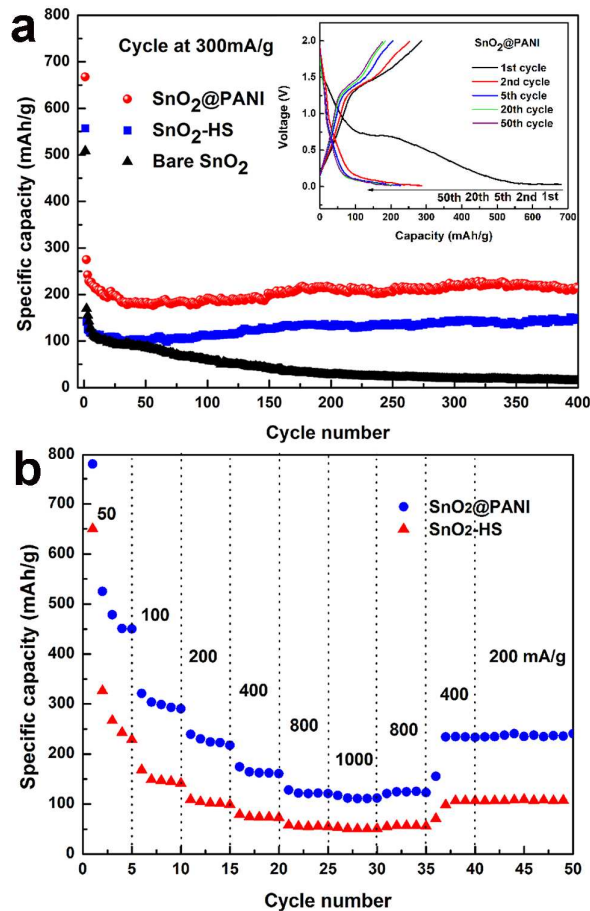


Fig. 5 (a) Cycling performances of bare SnO₂, SnO₂-HS and SnO₂@PANI anode electrodes. The inset shows the charge and discharge profiles of SnO₂@PANI anode electrodes in the 1st, 2nd, 5th, 20th and 50th cycles; (b) Rate performance of SnO₂@PANI nanocomposites at varied current densities.

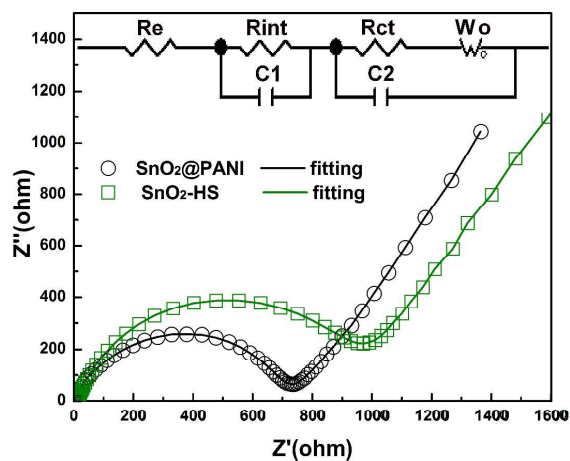


Fig. 6 EIS for SnO₂-HS and SnO₂@PANI core-shell composites anodes. The inset is the equivalent circuit used for the analysis of the impedance plots.

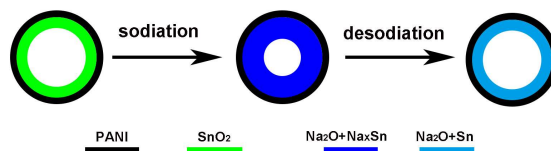


Fig. 7 Scheme of the role of PANI in alleviating the volume change of SnO₂-HS during the sodiation/desodiation reactions.

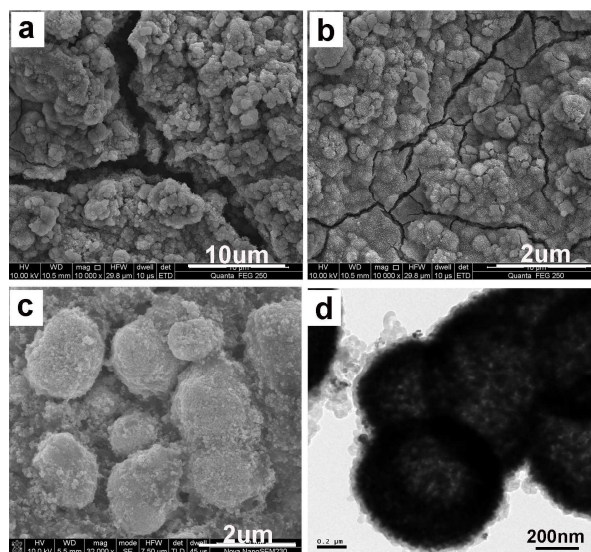


Fig. 8 SEM images of (a) bare SnO₂ electrode after 400 cycles; and (b,c) SnO₂@PANI electrode after 400 cycles; (d)TEM image of SnO₂@PANI composites after 400 cycles.